Accepted Manuscript

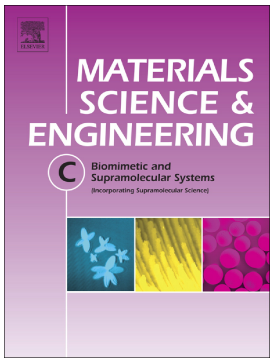

A voltammetric biosensor based on poly(o-methoxyaniline)-gold nanocomposite modified electrode for the simultaneous determination of dopamine and folic acid

D. Sangamithirai, S. Munusamy, V. Narayanan, A. Stephen

PII: S0928-4931(17)33844-4
DOI: doi:10.1016/j.msec.2018.05.070
Reference: MSC 8628

To appear in: *Materials Science & Engineering C*

Received date: 22 September 2017
Revised date: 25 April 2018
Accepted date: 23 May 2018

Please cite this article as: D. Sangamithirai, S. Munusamy, V. Narayanan, A. Stephen , A voltammetric biosensor based on poly(o-methoxyaniline)-gold nanocomposite modified electrode for the simultaneous determination of dopamine and folic acid. The address for the corresponding author was captured as affiliation for all authors. Please check if appropriate. Msc(2017), doi:10.1016/j.msec.2018.05.070

This is a PDF file of an unedited manuscript that has been accepted for publication. As a service to our customers we are providing this early version of the manuscript. The manuscript will undergo copyediting, typesetting, and review of the resulting proof before it is published in its final form. Please note that during the production process errors may be discovered which could affect the content, and all legal disclaimers that apply to the journal pertain.

ACCEPTED MANUSCRIPT

A Voltammetric Biosensor Based on Poly(o-methoxyaniline)-Gold Nanocomposite Modified Electrode for the Simultaneous Determination of Dopamine and Folic Acid

D. Sangamithirai[1], S. Munusamy[2], V. Narayanan[2], A. Stephen[1]*

[1]Materials Science Centre, Department of Nuclear Physics, University of Madras, Guindy Campus, Chennai 600025, India.

[2]Department of Inorganic Chemistry, University of Madras, Guindy Campus, Chennai 600025, India.

*Corresponding author: stephen_arum@hotmail.com

Phone: 044 22202802 Fax: 044 22351269

ACCEPTED MANUSCRIPT

ACCEPTED MANUSCRIPT

Abstract

Dopamine (DA) and Folic acid (FA) are co-existing compounds in biological fluids that plays a vital role in central nervous system and human metabolism. DA is an important neurotransmitter in the brain's neural circuits and its diminution often results in Parkinson's disease. Folate is another form of folic acid, which is known as one of the B vitamins. It is utilized as an additive by women during pregnancy in order to prevent the neural tube defects. The present study reports on the fabrication of electrochemical sensor for the simultaneous determination of DA and FA using poly(o-methoxyaniline)-gold (POMA-Au) nanocomposite. The POMA-Au nanocomposite was prepared via insitu chemical oxidative polymerization method and characterized using X-ray diffraction (XRD), high-resolution transmission electron microscopy (HRTEM) and X-ray photoelectron spectroscopy (XPS). The suitability of POMA-Au nanocomposite as a modifier for the electrocatalytic detection of DA and FA in aqueous solution was investigated by cyclic voltammetry (CV), differential pulse voltammetry (DPV) and chronoamperometry (CA) techniques. The fabricated POMA-Au/GCE sensor exhibited sharp and intense peaks towards the electro-oxidation of DA and FA as compared to bare electrode. The sensor exhibited the promising electron mediating behavior with well separated oxidation peaks with a potential difference of about 350.0 mV. The linear calibration plots of DA and FA were obtained from 10.0 to 300.0 μM and 0.5 to 900.0 μM with the detection limits of 0.062 μM and 0.090 μM, respectively. The reliability of this sensor was verified to be precise as well as sensitive for the determination of DA and FA in pharmaceutical samples and human urine samples.

Keywords: poly(o-methoxyaniline); gold nanoparticles; voltammetric sensor; dopamine; folic acid; simultaneous determination.

ACCEPTED MANUSCRIPT

1. Introduction

The development of electroanalytical methods that permits sensitive detection and quantification of electroactive compounds in biological fluids are of great importance in diagnosing and monitoring several diseases. In recent times, electrochemical techniques have been widely acknowledged as a feasible and inexpensive method for the detection of small bioanalytes with better sensitivity and fast response [1-3]. The neurotransmitter dopamine (DA) is a naturally occurring catecholamine, which is widely distributed in central nervous system for transmitting messages, to maintain hormonal balance, emotion control and also plays a vital role in human metabolism and cardiovascular systems [4, 5]. Abnormality and dysfunction of DA implicates many chronic ailments such as Schizophrenia, Parkinson's, Alzheimer's and addiction [6]. Folic acid (FA) is a water-soluble vitamin that is created in nature by plants and micro-organisms. An inadequate concentration of FA in body fluids is proven to be associated with the presence of neural tube defects in newborns, risk of colorectal cancer, psychiatric disorders and increasing risk of heart attack and stroke [7-10]. Since, DA and FA are coexisting in the biological fluids such as blood serum and urine, it is essential to develop a selective and sensitive method for the simultaneous determination of these electroactive species for analytical and clinical research. However, DA and FA exhibits overlapping oxidation potential at the surface of unmodified electrode due to their similar electrochemical responses which leads to the search of promising materials to address the problem.

The advent of conducting polymers (CPs) is a breakthrough in electroanalytical studies and they have been extensively used as modifiers in electrochemical sensors due to their promising charge transport properties and biocompatibility [11-14]. In recent times, poly(o-methoxyaniline) (POMA), a substituted derivative of polyaniline is studied for sensor

ACCEPTED MANUSCRIPT

applications, as it exhibits various special features including good solubility in organic solvents, excellent electrochemical redox behaviour even in neutral solutions, high biocompatibility and environmental stability [15-18]. Though POMA is a favourable mediator, the drawbacks such as electronic transfer resistance, poor specificity and sensitivity hinders its vital role in modification process [19]. Our previous works were shown an improvement in the sensing performances such as limit of detection, sensitivity and selectivity in the fabricated electrochemical sensors using conducting polymer nanocomposite with organic/inorganic counterparts [20-22]. Thus, the usage of nanoparticles as a composite material would be a propitious approach to improve the catalytic activity and sensing performance of POMA.

In the recent past, a burst of research activity has been dedicated to the progress of inorganic nanomaterials and are widely used in numerous fields based on their unique and promising features [23-28]. The utilization of inorganic nanoparticles in electrochemistry is proven to develop the electrochemical performance, which stands for their excellent electrocatalytic properties [29, 30]. Among various inorganic nanomaterials, gold (Au) nanoparticles are promising due to their superior properties, such as strong ability to bind and adsorb, high surface reaction activity and fast electron transfer rate which enable them to be a composite material to enrich the properties of CPs and making them as preferable mediators for electrochemical sensors [31-36]. The synthesis of gold nanoparticles and gold based polymer nanocomposite systems has attracted much attention owing to their influential role in novel applications. Zohara et al. reported on the bio-synthesis of optically tunable gold nanoparticles for the effective detection of mercuric ions by capitalizing upon the amalgamation tendency of mercury with gold [37]. Shan et al. developed a new gene delivery vector using dendrimer-entrapped gold nanoparticles, which exhibited higher gene transfection efficiency than that of dendrimers without gold nanoparticles [38]. Khan et al. studied the photocatalytic and

ACCEPTED MANUSCRIPT

antibacterial activity of biosynthesized gold nanoparticles. The synthesized gold particles were found to possess excellent antibacterial properties against both gram positive and gram negative bacteria and photocatalytic activity in terms of degrading methylene blue under ambient temperature [39]. Mendoza et al. investigated the bactericidal effect of gold-chitosan nanocomposite in coculture models of pathogenic bacteria. It was reported that, the prepared gold-chitosan colloid exhibited superior bactericidal ability against bacterial models without showing cytotoxicity on human cells at the tested concentrations [40]. Zhao et al. reported on the reliable dopamine (DA) sensor based on polythionine/gold nanoparticles (PTh/AuNPs) composite modified glassy carbon electrode (GCE). Compared with pure polythionine, the synthesized PTh/AuNPs exhibited enhanced electron transfer property, higher electroactive areas and more efficient electrocatalytic activity of DA [41]. The fabrication of PANI/Au nanocomposite modified nanoelectrode for sensitive dopamine nanosensor design was reported by Zhang et al. The modified nanoelectrode exhibited excellent electrocatalytic activity for the oxidation of ascorbic acid and dopamine in neutral pH solution [42].

Nanocomposite system consisting of poly(o-methoxyaniline) and gold nanoparticles would be a powerful choice, since it encompasses the special features of both the moieties and enable the system to be functionalized in modified sensors with improved sensitivity and selectivity. To the best of our knowledge, there are no reports available on the simultaneous determination of DA and FA using poly(o-methoxyaniline) and gold nanocomposite. With this concern, the present study focuses on the preparation of polymer nanocomposite using poly(o-methoxyaniline) and gold nanoparticles (POMA-Au) via insitu chemical oxidative polymerization method. The prepared nanocomposite was functionalized to modify glassy carbon electrode and designed as an electrochemical sensor for the simultaneous determination of two co-existing biomolecules such as DA and FA. POMA-Au/GCE showed an improved

ACCEPTED MANUSCRIPT

electrocatalytic activity towards the determination of DA and FA with enhanced oxidation currents when compared to bare GCE, POMA/GCE and Au/GCE. The catalytic ability of the designed sensor for the detection of DA and FA in real and pharmaceutical samples has also been studied using voltammetric method.

2. Experimental

2.1 Chemicals

Gold chloride ($HAuCl_4$) with 50% Au basis, o-anisidine with ≥ 99% purity, ammonium persulfate with ≥ 98% purity, β-napthalene sulfonic acid were received from Sigma Aldrich, trisodium citrate extrapure 99% purity from Finar reagents, India, were used for the synthesis. Dopamine (DA), folic acid (FA), sodium dihydrogen phosphate, disodium hydrogen phosphate was purchased from Sigma Aldrich. All the chemicals used were of analytical grade. Doubly distilled water was utilized to prepare all the solutions and to carry out the experiments.

2.2 Preparation of gold nanoparticles

Gold nanoparticles were synthesized by citrate reduction method [43]. In a typical procedure, 100 mL of 5 mM $HAuCl_4$ aqueous solution was prepared in a round-bottom flask and the solution was heated to boil under constant stirring. Subsequently, 10 mL of 125 mM trisodium citrate was added rapidly to the above solution. The reaction mixture was boiled for another 15 min during which the solution colour was changed from pale yellow to deep red. The deep red colour indicated the formation of gold nanoparticles. The obtained solution was continuously stirred and cooled down to room temperature.

ACCEPTED MANUSCRIPT

2.3 Preparation of poly(o-methoxyaniline)-gold (POMA-Au) nanocomposite

Poly(o-methoxyaniline)-gold (POMA-Au) nanocomposite was prepared by insitu chemical oxidative polymerization method. 6.16 mL (0.2 M) of o-methoxyaniline and 10.41 g (0.2 M) β-napthalene sulfonic acid was dissolved in distilled water and kept under magnetic stirring for 30 min. The amount of gold was taken in such a way that the composite would contain 10 wt% (i.e 0.616 g) of gold nanoparticles, and added to the acidified monomer solution and then allowed to stir for 30 min. The polymerization was initiated by adding aqueous solution of ammonium persulfate (0.1 M) dropwise to the above solution. After the addition of oxidant, the reaction was continued for 12 h at 0-5 °C. The dark green precipitate obtained from the reaction vessel was washed with water and methanol for several times and dried in air oven. Pure POMA was synthesized using the same procedure without the addition of gold nanoparticles.

2.4 Instrumentation

Cyclic voltammograms (CVs), differential pulse voltammograms (DPVs) and chronoamperograms (CAs) were obtained using CHI 1103A electrochemical workstation with a typical three-electrode cell arrangement. Glassy carbon electrode (GCE) with an electrode area of 0.07 cm^2 was used as working electrode, reference electrode was saturated calomel electrode (SCE) and the counter electrode was platinum wire. The X-ray diffraction patterns were recorded using GE X-ray diffraction system – XRD 303 TT with $CuK_{\alpha 1}$ radiation with a wavelength of 1.5406 Å. X-ray photoelectron spectroscopy experiments were done using DAR400-XM 1000 (OMICRON Nanotechnologies, Germany) coupled with Al anode as the X-ray source. High resolution transmission electron microscope images were obtained using PHILIPS CM200 transmission electron microscope instrument operating at 200 kV coupled with SAED facility.

ACCEPTED MANUSCRIPT

2.5 Fabrication of modified electrodes

Glassy carbon electrode (GCE) was polished with 0.3 and 0.05 μm alumina slurries on a silk polishing cloth to obtain a mirror-like electrode surface, rinsed with doubly distilled water, ultrasonicated for 10 min and then dried at room temperature. 3 mg of POMA-Au nanocomposite was dispersed in 1 mL of ethanol and sonicated for 30 min to attain a uniform solution. 2 μL of the solution was coated on the electrode surface to obtain POMA-Au-modified GCE (POMA-Au/GCE). For comparative analysis, 2 μL of POMA in ethanol (3 mg/mL) and 2 μL of Au nanoparticles in ethanol (3 mg/mL) was coated on GCE surface to obtain the POMA/GCE and Au/GCE, respectively.

2.6 Preparation of real samples

Pharmaceutical samples and human urine samples were taken for the determination of DA and FA. Standard addition method was used for estimating DA and FA concentration in the samples. Dopamine injection and folvite tablets were purchased from drugstore. Human urine sample was collected from Government Hospital, Chennai. The injection solution was diluted to 200 mL using deionized water, and then different quantity of diluted solution was transferred to volumetric flasks and then further diluted with phosphate buffer solution (pH 7.0). 10 mL of the prepared test solution was placed in an electrochemical cell and DPV experiment was performed. The purchased folvite tablets were well-grinded to a fine powder. The sample was weighed and mixed with 150 mL of deionized water and then ultra-sonicated for 15 min to get a clear solution. 100 μL of the solution was added with phosphate buffer solution (PBS, pH 7.0) to carry out the analysis. The human urine samples were diluted 10 times with PBS (pH 7.0) and used for analysis without any other treatment.

ACCEPTED MANUSCRIPT

3. Results and Discussion

3.1 Structural analysis

Fig.1 shows the XRD patterns of as-prepared gold nanoparticles and POMA-Au nanocomposite. The diffraction pattern of gold nanoparticles presented the face-centered cubic (fcc) structure with peaks at 38.1°, 44.4°, 64.5° and 77.7° corresponding to (111), (200), (220) and (311) planes, respectively (Fig. 1a). The observed pattern is in good agreement with the JCPDS card No. 04-0784 [44]. The average crystallite size of gold nanoparticles calculated using Scherrer's formula was ~ 5 nm. The XRD pattern of POMA-Au (Fig. 1b) showed the presence of both POMA (11.9° and 25.3°) [45] and Au (38.1°, 44.4°, 64.5° and 77.7°), confirming the formation of nanocomposite. The XRD pattern of nanocomposite clearly depicted the crystalline structure of gold nanoparticles even after the polymerization.

3.2 Morphology studies

The HRTEM images of as-prepared gold nanoparticles and POMA-Au nanocomposite with different magnifications are shown in Fig. 2. The micrographs of spherically shaped gold nanoparticles with an average particle size of ~5 nm is observed from Fig. 2(a & b). The formation of polymer matrix nanocomposite with POMA as the matrix phase with gold nanoparticles as the filler phase is evident from Fig. 2(c & d). The image of the composite at a resolution of 2 nm is shown in Fig. 2(e), at which the fringes in the particle are clearly visible. The d-spacing values were calculated as 0.236, 0.204 and 0.16 nm, corresponding to (111), (200) and (220) planes of gold nanoparticles. This confirms that the particles observed in the POMA matrix are gold nanoparticles.

The selected area electron diffraction (Fig. 2f) of POMA-Au nanocomposite shows the high crystalline nature of gold nanoparticles in the composite. The d-spacing values were

ACCEPTED MANUSCRIPT

measured from the observed SAED pattern which signifies (111), (200), (220) and (311) planes of gold. The obtained planes correlate well to the planes of face centered cubic structure of gold and the results are in good agreement with XRD report.

3.3 X-ray photoelectron spectroscopy (XPS)

Fig. 3 shows the XPS spectra of POMA-Au nanocomposite. The presence of carbon, nitrogen, oxygen, sulfur and gold (Fig. 3a) is revealed from the survey spectrum without any other impurities, thus indicating the purity of the sample. The C 1s spectrum was deconvoluted into 3 peaks at 284.5, 286.1 and 288.5 eV as shown in Fig. 3b. The peak observed at the binding energy of 284.5 eV is attributed to C—C/C—H bond. The presence of peak at 286.1 eV is associated to C—N/C=N/C—S bonding, while the peak at 288.5 eV is due to —C═N^+ bond [46-48]. The core level spectrum of N 1s energy level showed the presence of 3 peaks, as seen in Fig. 3c. The peaks observed at the binding energies of 399.3 eV is due to the presence of —NH— (neural N at the POMA ring) [49]. Further, the peaks at 400.5 eV and 402.4 eV are attributed to the presence of cationic nitrogen atoms (=N^+) and the protonated amine units (—NH^+—) in POMA [50]. The deconvoluted XPS spectrum of O 1s (Fig. 3d) exhibited the presence of OH bonds, C=O bonds, O=S of SO_3^- groups of β-NSA in the composites, C—O—C and C—O—H environments [51-54] at the binding energies of 530.0, 531.1 532.3, 533.5 and 534.7 eV, respectively. As seen in Fig. 3(e), the core level spectrum of S (2p) exhibited the double peak feature at the binding energies of 163.9 and 168.8 eV associated to $2P_{3/2}$ and $2P_{1/2}$ energy levels. The core level spectrum of gold (Fig. 3f) showed the presence of $4f_{7/2}$ and $4f_{5/2}$ at the binding energies of 84.24 eV and 87.84 eV, respectively with a difference of 3.6 eV. The Au $4f_{7/2}$ peak was shifted towards higher binding energy by 0.2 eV when compared to the original binding energy value of metallic gold (84.04 eV). This shift in binding energy towards

ACCEPTED MANUSCRIPT

higher value is attributed to the binding of gold nanoparticles to polymer and also due to the particle size effect [55, 56]. Thus, XPS results confirm the binding of gold nanoparticles to POMA and thus signify the formation of POMA-Au nanocomposite.

3.4 Electrochemical characterizations

The electroactive surface area of the working electrode was determined using $[Fe(CN)_6]^{3-/4-}$ as redox probes by cyclic voltammetry (CV). Fig. 4A shows the CVs of bare GCE and the composite POMA-Au/GCE recorded with 1 mM $[Fe(CN)_6]^{3-/4-}$ in 0.1 M KCl at 50 mV/s. A pair of redox peaks was observed at the surface of bare GCE (curve a) with a peak separation of 285 mV. On the other side, POMA-Au/GCE exhibited a highly intense redox peaks with ΔE_p value of ~ 135 mV smaller while compared to bare GCE. The observed minimal ΔE_p and the corresponding improvement in the redox peak currents at POMA-Au/GCE indicates the good electron transfer kinetics and large active surface area of POMA and Au nanoparticles. The active surface area of the modified electrode was calculated using Randles-Sevcik equation (equation 1),

$$i_p = (2.69\ x\ 10^5) n^{3/2} D^{1/2} C A \nu^{1/2} \quad \text{---------- (1)}$$

where, *A* represents the microscopic area of the working electrode, *n* stands for the number of electrons involved in the reaction (*n* = 1), *D* is the diffusion coefficient (*D* = 6.70 x 10^{-6} cm^2/s), *C* is the concentration of $[Fe(CN)_6]^{3-/4-}$ (1 mM) and *v* is the scan rate (V/s). From the plot of i_{peak} and square root of the scan rate ($\nu^{1/2}$) (inset of Fig. 4B), the surface areas of bare GCE and POMA-Au/GCE were calculated as 3.85 mm^2 and 9.96 mm^2, respectively. The observed results show that the composite of POMA and Au nanoparticles have significantly increased the surface area of the working electrode.

ACCEPTED MANUSCRIPT

3.5 Electrochemical behaviors of DA and FA

Cyclic voltammetry was used to study the electrochemical behaviours of DA and FA at POMA-Au/GCE in phosphate buffer solution (PBS) with pH 7.0. Fig. S1and S2 (supplementary information) shows the effect of pH solution towards the determination of DA and FA. Based on the results of pH analysis, PBS (pH 7.0) was chosen as the optimal supporting electrolyte for the electrochemical determination of DA and FA and thus used in subsequent studies. Fig. 5A shows the CV responses of 1 mM DA at bare GCE (curve a), POMA/GCE (curve b), Au/GCE (curve c) and POMA-Au/GCE (curve d). The oxidation-reduction potentials and catalytic currents for DA reaction are listed in **Table 1**. As shown in Fig. 5A, an ill-defined redox behavior with high over-potential was observed at the surface of bare GCE with ΔE_p ~ 960 mV. This indicates the slow electron transfer rate owing to the fouling of bare electrode surface by the adsorption of DA oxidation products. A pair of well-defined redox peaks was recorded with a systematic increment in the peak currents on modification of nanomaterials suggesting the efficient detection of DA at the surface of modified electrodes. However, POMA-Au/GCE exhibited a well-defined redox peaks with the oxidation and reduction potential at 0.33 V and -0.02 V (ΔE_p ~ 350 mV), respectively with higher current values in comparison to bare GCE, POMA/GCE and Au/GCE. The combination of POMA and Au nanoparticles facilitated the charge transfer ability and thus improved the electron rate between DA and working electrode. The effect of scan rate on the electrochemical behavior of DA at POMA-Au/GCE showed the proportionality of peak currents with the square root of the scan rate in the range of 5 to 200 mV/s (Fig. 5B). The corresponding linear regression equation was deduced as I_{pa} (μA) = 2.71 $\nu^{1/2}$ (mV/s) + 1.96 (r^2 = 0.990) and I_{pc} (μA) = –2.34 $\nu^{1/2}$ (mV/s) – 1.73 (r^2 = 0.993), which suggests that the POMA-Au/GCE is

ACCEPTED MANUSCRIPT

diffusion – controlled process. The calibration plot of oxidation and reduction peak potential (E_{pa} and E_{pc}) with ln ν also displayed a linear relationship with the regression equations as E_{pa} = 0.004 ln ν + 0.313 (r^2 = 0.992) and E_{pc} = –0.003 ln ν – 0.026 (r^2 = 0.991). The electrochemical parameters such as electron transfer coefficient (α), the electron transfer number (n) and the standard electron transfer rate constant (k_s) of DA at POMA-Au/GCE were calculated based on Laviron's equations [57].

$$E_{pa} = \frac{E^{o\prime} + 2.3\ RT}{(1-\alpha)nF\ log\nu} \text{ ---------- (2)}$$

$$E_{pc} = \frac{E^{o\prime} - 2.3\ RT}{\alpha nF\ log\nu} \text{ ---------- (3)}$$

$$\log k_s = \alpha \log(1-\alpha) + (1-\alpha)log\alpha - \log\left(\frac{RT}{nF\nu}\right) - \frac{(1-\alpha)\alpha nF\Delta E_p}{2.3\ RT} \text{ ---------- (4)}$$

Using equations (2) and (3), the values of α and n were evaluated as 0.63 and 2.3. Then, the average value of k_s was calculated to be 0.75 s^{-1}.

To evaluate the limit of detection (LOD) of the fabricated sensor, differential pulse voltammograms (DPVs) were recorded with different concentrations of DA at POMA-Au/GCE. As shown in Fig. 5C, DA showed the oxidation peak at a potential of ~ 0.3 V. The peak current was improved with the increasing concentration of DA in the range of 10.0 to 300.0 µM. The experimental plot of peak current versus DA concentration exhibited a linear relationship with the regression equation of I_{pa} (µA) = 0.06 C_{DA} (µM) + 5.76 (r^2 = 0.998), as shown in Fig. 5D. On analyzing the results, limit of detection (LOD) of this system was calculated as 0.062 µM (LOD = $3S_b/q$; where S_b is the standard deviation of the blank signal and q is the slope of the calibration curve). The performance of the POMA-Au/GCE is in comparison with the other modified electrodes as summarized in **Table 2**. It can be seen that the developed POMA-

ACCEPTED MANUSCRIPT

Au/GCE has comparable sensing performance for the detection of DA when compared to other electrodes reported in the literature [58-63].

For the electro-oxidation of FA (Fig. 6A), a broad and low-intense oxidation peak was observed with a potential of ~ 0.75 V at the surface of bare GCE (curve a). A well-defined oxidation peak with improved peak current was recorded on modifying the electrode surface with POMA and Au nanoparticles (curves b & c), respectively. In contrast, POMA-Au/GCE (curve d) exhibited highly intense peak at an oxidation potential of ~ 0.68 V, which is an evidence for the facile electron transfer reaction and improved electrocatalytic oxidation. The standard rate constant (k_s) values of the modified electrodes at the surface of POMA/GCE, Au/GCE and POMA-Au/GCE were measured using the following equation [64, 65].

$$k_s = 1.11\, D^{1/2}(E_p - E_{p/2})^{-1/2}\, \nu^{1/2} \quad \text{---------- (5)}$$

where, D is the diffusion coefficient (D = 2.13 x 10^{-5} cm^2/s), E_p is the oxidation peak potential; $E_{p/2}$ is the half-wave oxidation peak potential and ν is the scan rate. For the electro-oxidation of FA, the k_s values were calculated as 0.58 x 10^{-3}, 0.67 x 10^{-3} and 2.0 x 10^{-3} cm/s at the surface of POMA/GCE, Au/GCE and POMA-Au/GCE, respectively. The obtained values indicate that, the fast electron transfer for the electro-oxidation of FA was achieved at the surface of POMA-Au/GCE than that of POMA/GCE and Au/GCE. In addition, a good linear relationship was observed between the anodic peak current and the square root of the scan rate in the range of 5 to 200 mV/s (I_{pa} (μA) = 2.49 $\nu^{1/2}$ (mV/s) + 16.40 (r^2 = 0.993)) (Fig. 6B). The observed results demonstrate that the electrode reaction is controlled by diffusion process. The plot of anodic peak potential and ln ν, exhibited a linear relationship with a regression equation of, E_{pa} = 0.016 ln ν + 0.643 (r^2 = 0.992, E_{pa} in V, ν in mVs^{-1}). On using the following equation [66],

ACCEPTED MANUSCRIPT

$$E_{pa} = E^0 + m\,[0.78 + ln\,(D^{\frac{1}{2}} K_s^{-1}) - 0.5\,ln\,m] + \frac{m}{2} ln(v) \quad \text{---------- (6)}$$

with, $m = \frac{RT}{(1-\alpha)n\alpha F}$

where R is the gas constant, T is the temperature (K), n is the electron transfer number, α is the electron transfer coefficient and F is the Faraday constant. The value of m was determined as 0.051 and thus, the electron transfer coefficient (α) for the electro-oxidation of FA is approximately 0.48.

Fig. 6C shows the DPV curves for different concentrations of FA at POMA-Au/GCE. The peak current was increased with the concentrations of FA over the range of 0.5 to 900.0 μM. The calibration plot of peak current was in linear proportion to the concentration of FA (Fig. 6D). The corresponding regression equation deduced from the plot was I_{pa} (μA) = 0.024 C_{FA} (μM) + 12.10 (r^2 = 0.994) and the limit of detection was 0.090 μM, which is found to be comparable and better than the previously reported values as shown in **Table 3** [3, 67-71].

3.6 Simultaneous determination of DA and FA

The most significant objective of the present study is the simultaneous determination of DA and FA at POMA-Au/GCE, since the oxidative potentials of the two compounds are very close to each other. Thus, we have investigated the simultaneous determination and sensitivity of the analytes in the presence of other compound using DPV. Fig. 7 shows the DPVs obtained from the mixture of both the analytes with different concentrations. Two well-defined oxidation peaks were observed in a mixture of DA and FA solution, with highly resolved signals and a large peak potential separation of about 350.0 mV at the surface of POMA-Au/GCE. On simultaneously increasing the concentration of DA and FA, the corresponding anodic peak

ACCEPTED MANUSCRIPT

currents also increased linearly. From the plot between the concentration of analytes and peak current, a linear relationship was observed over the concentration range of 10.0 to 300.0 μM for DA and 0.5 to 900.0 μM for FA. The corresponding linear regression equation was I_{pa} (μA) = 0.052 C_{DA} (μM) + 5.98 (r^2 = 0.997) (inset (i) of Fig.7) and I_{pa} (μA) = 0.03 C_{FA} (μM) + 9.0 (r^2 = 0.997) (inset (ii) of Fig.7) for DA and FA, respectively. From the obtained data, it is found that the sensitivities of the modified electrodes for the determination of DA and FA are almost same even in the presence of other compound. This indicates the electro-oxidation process of DA and FA at POMA-Au/GCE is non-overlapping and thus simultaneous detection of these species is attainable without much change in the sensitivity parameters.

3.7 Interference evaluation of DA and FA

DPVs were recorded at the surface of POMA-Au/GCE to study the electro-oxidation process by varying the concentration of one compound while keeping the other as constant. Fig. 8A shows the DPV curves with different concentrations of DA mixed with a constant amount of FA (200.0 μM). The peak current of FA was found to be almost similar for each addition of DA in the mixture solution which depicts the good resolution of the two species at the surface of fabricated sensor. The experimental plot of DA exhibited a linear range of 50.0 to 300.0 μM and the regression equation was I_{pa} (μA) = 0.042 C_{DA} (μM) + 15.32 (r^2 = 0.997). Similarly, the DPV experiment was conducted with a mixture solution containing constant amount of DA (30.0 μM) with various concentrations of FA (Fig. 8B). The calibration plot of peak current with concentration of FA was found to be proportional in the range of 350.0 to 900.0 μM of FA and the corresponding regression equation was determined to be I_{pa} (μA) = 0.02 C_{FA} (μM) + 16.02 (r^2 = 0.998).

ACCEPTED MANUSCRIPT

3.8 Chronoamperometric studies

Chronoamperometric measurements were carried out to investigate the electrode processes at the surface of modified electrodes. Chronoamperometry studies of DA were done by fixing the working electrode potential at 0.3 V for different concentrations of DA (0.1, 0.3, 0.5, 0.7 and 0.9 mM) and the results are shown in Fig. 9A. The diffusion coefficient (*D*) of DA was determined using the Cottrell equation [72],

$$I = nFAD^{\frac{1}{2}}C\pi^{\frac{-1}{2}}t^{\frac{-1}{2}} \text{ ---------- (7)}$$

where, *C* is the concentration (mol cm^{-3}) of DA, and all other parameters are the same as stated in the above equation. The plots of current (I) versus $t^{-1/2}$ were constructed for different concentrations of DA (inset (i) of Fig. 9A) in 0.1 M PBS (pH 7.0). The slope values of the resultant straight lines were plotted with concentrations of DA (inset (ii) of Fig. 9A). Using the Cottrell equation (equation 7), the mean value of diffusion coefficient (D) was calculated to be 6.796 x 10^{-6} cm^2/s. In a similar way, the D value of FA was evaluated as 2.13 x 10^{-5} cm^2/s, by fixing the electrode potential at 0.68 V, then carried out the above-mentioned steps and the obtained results are shown in Fig. 9B.

3.9 Reproducibility and stability

The reproducibility of the POMA-Au/GCE sensor was evaluated by determining the peak currents of 15 successive measurements in the binary mixture solution of 0.2 mM DA and 0.1 mM FA using DPV technique. The relative standard deviation of 3.17% and 3.52% was obtained for DA and FA, respectively. The stability of the modified electrode was tested using DPV technique with phosphate buffer solution containing 100 µM of DA and FA. After 25 continuous runs, the recorded curves showed a loss of 1.32% and 1.17% from its initial value.

ACCEPTED MANUSCRIPT

The storage stability of the fabricated electrode was also tested by preserving the electrode in a refrigerator (4 °C) for 2 weeks. The peak current values of DA and FA were decreased by 5.2% and 4.8%, respectively at the surface of POMA-Au/GCE. The observed results suggest the good reproducibility and stability without any surface fouling of the fabricated electrode.

3.10 Analysis of DA and FA in real samples

The reliability of the proposed method was verified by applying POMA-Au/GCE for the determination of DA and FA in pharmaceutical samples and in human urine samples using standard addition method. The analytical results obtained for pharmaceutical samples are given in **Table 4**, showing the recovery rate in the range of 97.3% to 100.2% for DA in dopamine injections and 97.1% to 99.6% for FA in folvite tablets.

The applicability of the proposed sensor was also analyzed for the determination of DA and FA in human urine samples and the corresponding results are summarized in **Table 5**. The recovery of the samples was ranged from 97.5% to 99.3% for DA and 96.2% to 99.0% for FA. The results indicate the effectiveness of the proposed sensor towards the determination of DA and FA in pharmaceutical and in human urine samples with good recovery rate.

4. Conclusion

A sensitive electrochemical sensor was fabricated using poly(o-methoxyaniline)-gold (POMA-Au) nanocomposite for the simultaneous determination of dopamine (DA) and folic acid (FA). The POMA-Au/GCE exhibited a favorable electrochemical behavior for the oxidation of DA and FA with enhanced current response together with lowering the over-potentials and also separated the overlapping peaks of these species with high resolution. The sensor incorporates the excellent catalytic activity and biocompatibility of POMA with the large surface area and high electrical conductivity of gold nanoparticles which was used not only to improve the

ACCEPTED MANUSCRIPT

sensing performance but also to increase the stability of the sensor. Besides, the POMA-Au sensor exhibited wide linear range and low detection limit for the determination of DA (10.0 to 300.0 μM & 0.062 μM) and FA (0.5 to 900.0 μM & 0.090 μM), respectively. The proposed nanocomposite sensor is shown to be useful for the determination of DA and FA in pharmaceutical and human urine samples.

Acknowledgements

One of the authors D. Sangamithirai acknowledges DST-INSPIRE, India for the award of fellowship. The authors thank NCNSNT, University of Madras for HRTEM characterization.

References

[1] V.K. Gupta, R. Jain, K. Radhapyari, N. Jadon, S. Agarwal, Voltammetric techniques for the assay of pharmaceuticals—A review, Analytical Biochemistry, 408 (2011) 179-196.
[2] J. Wu, J. Suls, W. Sansen, Amperometric determination of ascorbic acid on screen-printing ruthenium dioxide electrode, Electrochemistry Communications, 2 (2000) 90-93.
[3] N. Lavanya, E. Fazio, F. Neri, A. Bonavita, S.G. Leonardi, G. Neri, C. Sekar, Electrochemical sensor for simultaneous determination of ascorbic acid, uric acid and folic acid based on Mn-SnO2 nanoparticles modified glassy carbon electrode, Journal of Electroanalytical Chemistry, 770 (2016) 23-32.
[4] B.E. Leonard, Biochemical Basis of Neuropharmacology (8th Edition). J. R. Cooper, F. E. Bloom and R. H. Roth. Oxford University Press: Oxford, 2002. ISBN 0-19-514007-9, Human Psychopharmacology: Clinical and Experimental, 19 (2004) 67-67.
[5] P. Damier, E.C. Hirsch, Y. Agid, A.M. Graybiel, The substantia nigra of the human brainII. Patterns of loss of dopamine-containing neurons in Parkinson's disease, Brain, 122 (1999) 1437-1448.
[6] R.M. Wightman, L.J. May, A.C. Michael, Detection of Dopamine Dynamics in the Brain, Analytical Chemistry, 60 (1988) 769A-793A.
[7] S.N. Young, The 1989 Borden Award Lecture. Some effects of dietary components (amino acids, carbohydrate, folic acid) on brain serotonin synthesis, mood, and behavior, Canadian Journal of Physiology and Pharmacology, 69 (1991) 893-903.
[8] C.M. Ulrich, Nutrigenetics in cancer research--folate metabolism and colorectal cancer, J Nutr, 135 (2005) 2698-2702.
[9] L.E. Mitchell, N.S. Adzick, J. Melchionne, P.S. Pasquariello, L.N. Sutton, A.S. Whitehead, Spina bifida, Lancet, 364 (2004) 1885-1895.
[10] B.B. Prasad, M.P. Tiwari, R. Madhuri, P.S. Sharma, Development of a highly sensitive and selective hyphenated technique (molecularly imprinted micro-solid phase extraction fiber–molecularly imprinted polymer fiber sensor) for ultratrace analysis of folic acid, Analytica Chimica Acta, 662 (2010) 14-22.
[11] H. Shirakawa, E.J. Louis, A.G. MacDiarmid, C.K. Chiang, A.J. Heeger, Synthesis of electrically conducting organic polymers: halogen derivatives of polyacetylene, (CH), Journal of the Chemical Society, Chemical Communications, DOI 10.1039/c39770000578(1977) 578-580.
[12] M. Ates, A review study of (bio)sensor systems based on conducting polymers, Materials Science and Engineering: C, 33 (2013) 1853-1859.

ACCEPTED MANUSCRIPT

[13] X. Li, Y. Wang, X. Yang, J. Chen, H. Fu, T. Cheng, Conducting polymers in environmental analysis, TrAC Trends in Analytical Chemistry, 39 (2012) 163-179.
[14] H. Karimi-Maleh, F. Tahernejad-Javazmi, N. Atar, M.L. Yola, V.K. Gupta, A.A. Ensafi, A Novel DNA Biosensor Based on a Pencil Graphite Electrode Modified with Polypyrrole/Functionalized Multiwalled Carbon Nanotubes for Determination of 6-Mercaptopurine Anticancer Drug, Industrial & Engineering Chemistry Research, 54 (2015) 3634-3639.
[15] R. Aitout, A. Belgaid, L. Makhloufi, B. Saidani, Synthesis of conducting poly-ortho-methoxy-aniline films onto an inert support (Plexiglas) and their modification with gold by cementation: Electrocatalytic tests versus oxidation of hydrazine and proton reduction, Reactive and Functional Polymers, 66 (2006) 373-377.
[16] J.-B. Raoof, S.R. Hosseini, S. Rezaee, Preparation of Pt/poly(2-Methoxyaniline)/multi-walled carbon nanotube nanocomposite and its application for electrocatalytic oxidation of methanol, Journal of Molecular Liquids, 200, Part B (2014) 196-204.
[17] L. Komsiyska, T. Tsacheva, V. Tsakova, Electrochemical formation and copper modification of poly-o-methoxyaniline, Thin Solid Films, 493 (2005) 88-95.
[18] M. Mazur, A. Michota-Kamińska, J. Bukowska, Surface-catalyzed growth of poly(2-methoxyaniline) on gold, Electrochimica Acta, 52 (2007) 5669-5676.
[19] L. Komsiyska, V. Tsakova, Ascorbic Acid Oxidation at Nonmodified and Copper-Modified Polyaniline and Poly-ortho-methoxyaniline Coated Electrodes, Electroanalysis, 18 (2006) 807-813.
[20] D. Sangamithirai, V. Narayanan, B. Muthuraaman, A. Stephen, Investigations on the performance of poly(o-anisidine)/graphene nanocomposites for the electrochemical detection of NADH, Materials Science and Engineering: C, 55 (2015) 579-591.
[21] D. Sangamithirai, S. Munusamy, V. Narayanan, A. Stephen, Fabrication of neurotransmitter dopamine electrochemical sensor based on poly(o-anisidine)/CNTs nanocomposite, Surfaces and Interfaces, 4 (2016) 27-34.
[22] D. Sangamithirai, S. Munusamy, V. Narayanan, A. Stephen, A strategy to promote the electroactive platform adopting poly(o-anisidine)-silver nanocomposites probed for the voltammetric detection of NADH and dopamine, Materials Science and Engineering: C, 80 (2017) 425-437.
[23] C. Dhand, N. Dwivedi, X.J. Loh, A.N. Jie Ying, N.K. Verma, R.W. Beuerman, R. Lakshminarayanan, S. Ramakrishna, Methods and strategies for the synthesis of diverse nanoparticles and their applications: a comprehensive overview, RSC Advances, 5 (2015) 105003-105037.
[24] X.J. Loh, T.-C. Lee, Q. Dou, G.R. Deen, Utilising inorganic nanocarriers for gene delivery, Biomaterials Science, 4 (2016) 70-86.
[25] Q.Q. Dou, C.P. Teng, E. Ye, X.J. Loh, Effective near-infrared photodynamic therapy assisted by upconversion nanoparticles conjugated with photosensitizers, International Journal of Nanomedicine, 10 (2015) 419-432.
[26] B.M. Teo, D.J. Young, X.J. Loh, Magnetic Anisotropic Particles: Toward Remotely Actuated Applications, Particle & Particle Systems Characterization, 33 (2016) 709-728.
[27] E. Ye, M.D. Regulacio, M.S. Bharathi, H. Pan, M. Lin, M. Bosman, K.Y. Win, H. Ramanarayan, S.-Y. Zhang, X.J. Loh, Y.-W. Zhang, M.-Y. Han, An experimental and theoretical investigation of the anisotropic branching in gold nanocrosses, Nanoscale, 8 (2016) 543-552.
[28] K. Huang, Q. Dou, X.J. Loh, Nanomaterial mediated optogenetics: opportunities and challenges, RSC Advances, 6 (2016) 60896-60906.
[29] K.Z. Brainina, L.G. Galperin, E.V. Vikulova, Electrochemistry of metal nanoparticles: the effect of substrate, Journal of Solid State Electrochemistry, 16 (2012) 2357-2363.
[30] B. Šljukić, R. Baron, C. Salter, A. Crossley, R.G. Compton, Combinatorial electrochemistry using metal nanoparticles: From proof-of-concept to practical realisation for bromide detection, Analytica Chimica Acta, 590 (2007) 67-73.

ACCEPTED MANUSCRIPT

[31] H.Y. Jia, Y. Liu, X.J. Zhang, L. Han, L.B. Du, Q. Tian, Y.C. Xu, Potential Oxidative Stress of Gold Nanoparticles by Induced-NO Releasing in Serum, Journal of the American Chemical Society, 131 (2009) 40-41.
[32] M.-C. Daniel, D. Astruc, Gold Nanoparticles: Assembly, Supramolecular Chemistry, Quantum-Size-Related Properties, and Applications toward Biology, Catalysis, and Nanotechnology, Chemical Reviews, 104 (2004) 293-346.
[33] S. Guo, E. Wang, Synthesis and electrochemical applications of gold nanoparticles, Analytica Chimica Acta, 598 (2007) 181-192.
[34] C.M. Welch, R.G. Compton, The use of nanoparticles in electroanalysis: a review, Analytical and Bioanalytical Chemistry, 384 (2006) 601-619.
[35] J. Li, X.-Q. Lin, Electrodeposition of gold nanoclusters on overoxidized polypyrrole film modified glassy carbon electrode and its application for the simultaneous determination of epinephrine and uric acid under coexistence of ascorbic acid, Analytica Chimica Acta, 596 (2007) 222-230.
[36] T. Del Castillo-Castro, E. Larios-Rodriguez, Z. Molina-Arenas, M.M. Castillo-Ortega, J. Tanori, Synthesis and characterization of metallic nanoparticles and their incorporation into electroconductive polymer composites, Composites Part A: Applied Science and Manufacturing, 38 (2007) 107-113.
[37] N. Zohora, D. Kumar, M. Yazdani, V.M. Rotello, R. Ramanathan, V. Bansal, Rapid colorimetric detection of mercury using biosynthesized gold nanoparticles, Colloids and Surfaces A: Physicochemical and Engineering Aspects, 532 (2017) 451-457.
[38] Y. Shan, T. Luo, C. Peng, R. Sheng, A. Cao, X. Cao, M. Shen, R. Guo, H. Tomás, X. Shi, Gene delivery using dendrimer-entrapped gold nanoparticles as nonviral vectors, Biomaterials, 33 (2012) 3025-3035.
[39] A.U. Khan, Q. Yuan, Y. Wei, G.M. Khan, Z.U.H. Khan, S. Khan, F. Ali, K. Tahir, A. Ahmad, F.U. Khan, Photocatalytic and antibacterial response of biosynthesized gold nanoparticles, Journal of Photochemistry and Photobiology B: Biology, 162 (2016) 273-277.
[40] G. Mendoza, A. Regiel-Futyra, V. Andreu, V. Sebastián, A. Kyzioł, G. Stochel, M. Arruebo, Bactericidal Effect of Gold–Chitosan Nanocomposites in Coculture Models of Pathogenic Bacteria and Human Macrophages, ACS Applied Materials & Interfaces, 9 (2017) 17693-17701.
[41] C. Zhao, Z. Jiang, X. Cai, L. Lin, X. Lin, S. Weng, Ultrasensitive and reliable dopamine sensor based on polythionine/AuNPs composites, Journal of Electroanalytical Chemistry, 748 (2015) 16-22.
[42] Y. Zhang, L. Lin, Z. Feng, J. Zhou, Z. Lin, Fabrication of a PANI/Au nanocomposite modified nanoelectrode for sensitive dopamine nanosensor design, Electrochimica Acta, 55 (2009) 265-270.
[43] A. Dey, A. Kaushik, S.K. Arya, S. Bhansali, Mediator free highly sensitive polyaniline-gold hybrid nanocomposite based immunosensor for prostate-specific antigen (PSA) detection, Journal of Materials Chemistry, 22 (2012) 14763-14772.
[44] A.N. Mishra, S. Bhadauria, M.S. Gaur, R. Pasricha, B.S. Kushwah, Synthesis of Gold Nanoparticles by Leaves of Zero-Calorie Sweetener Herb (Stevia rebaudiana) and Their Nanoscopic Characterization by Spectroscopy and Microscopy, International Journal of Green Nanotechnology: Physics and Chemistry, 1 (2010) P118-P124.
[45] D. Patil, Y.-K. Seo, Y.K. Hwang, J.-S. Chang, P. Patil, Humidity sensing properties of poly(o-anisidine)/WO3 composites, Sensors and Actuators B: Chemical, 128 (2008) 374-382.
[46] L. Ruangchuay, J. Schwank, A. Sirivat, Surface degradation of α-naphthalene sulfonate-doped polypyrrole during XPS characterization, Applied Surface Science, 199 (2002) 128-137.
[47] High Resolution XPS of Organic Polymers: The Scienta ESCA300 Database (Beamson, G.; Briggs, D.), Journal of Chemical Education, 70 (1993) A25.
[48] G.V. Ouedraogo, D. Benlian, L. Porte, X-ray photoelectron spectroscopy of phthalocyanine compounds, The Journal of Chemical Physics, 73 (1980) 642-647.
[49] J.-W. Jeon, Y. Ma, J.F. Mike, L. Shao, P.B. Balbuena, J.L. Lutkenhaus, Oxidatively stable polyaniline:polyacid electrodes for electrochemical energy storage, Physical Chemistry Chemical Physics, 15 (2013) 9654-9662.

ACCEPTED MANUSCRIPT

[50] X.L. Wei, M. Fahlman, A.J. Epstein, XPS Study of Highly Sulfonated Polyaniline, Macromolecules, 32 (1999) 3114-3117.
[51] H. Deng, L. Yao, Q.-A. Huang, Q. Su, J. Zhang, F. Zhang, G. Du, Facile assembly of a S@carbon nanotubes/polyaniline/graphene composite for lithium-sulfur batteries, RSC Advances, 7 (2017) 9819-9825.
[52] S.A. Ansari, N. Parveen, T.H. Han, M.O. Ansari, M.H. Cho, Fibrous polyaniline@manganese oxide nanocomposites as supercapacitor electrode materials and cathode catalysts for improved power production in microbial fuel cells, Physical Chemistry Chemical Physics, 18 (2016) 9053-9060.
[53] E. Binkauskienė, V. Jasulaitienė, A. Lugauskas, Effect of Aspergillus niger Tiegh. L-10 on the physical and chemical properties of a polyaniline coating in the growth substrate, Synthetic Metals, 159 (2009) 1365-1368.
[54] H. Peng, G. Ma, K. Sun, J. Mu, X. Zhou, Z. Lei, A novel fabrication of nitrogen-containing carbon nanospheres with high rate capability as electrode materials for supercapacitors, RSC Advances, 5 (2015) 12034-12042.
[55] K. Szczepanowicz, J. Stefanska, R.P. Socha, P. Warszynski, Preparation of silver nanoparticles via chemical reduction and their antimicrobial activity, Physicochem Probl Miner Process, 45 (2010) 85-98.
[56] S. Shanmugam, B. Viswanathan, T.K. Varadarajan, Photochemically reduced polyoxometalate assisted generation of silver and gold nanoparticles in composite films: a single step route, Nanoscale Research Letters, 2 (2007) 175-183.
[57] E. Laviron, General expression of the linear potential sweep voltammogram in the case of diffusionless electrochemical systems, Journal of Electroanalytical Chemistry and Interfacial Electrochemistry, 101 (1979) 19-28.
[58] W. Zhu, T. Chen, X. Ma, H. Ma, S. Chen, Highly sensitive and selective detection of dopamine based on hollow gold nanoparticles-graphene nanocomposite modified electrode, Colloids and Surfaces B: Biointerfaces, 111 (2013) 321-326.
[59] D. Yuan, S. Chen, R. Yuan, J. Zhang, X. Liu, An ECL sensor for dopamine using reduced graphene oxide/multiwall carbon nanotubes/gold nanoparticles, Sensors and Actuators B: Chemical, 191 (2014) 415-420.
[60] J. Hou, C. Xu, D. Zhao, J. Zhou, Facile fabrication of hierarchical nanoporous AuAg alloy and its highly sensitive detection towards dopamine and uric acid, Sensors and Actuators B: Chemical, 225 (2016) 241-248.
[61] H. Yin, K. Shang, X. Meng, S. Ai, Voltammetric sensing of paracetamol, dopamine and 4-aminophenol at a glassy carbon electrode coated with gold nanoparticles and an organophillic layered double hydroxide, Microchimica Acta, 175 (2011) 39.
[62] J. Li, J. Yang, Z. Yang, Y. Li, S. Yu, Q. Xu, X. Hu, Graphene-Au nanoparticles nanocomposite film for selective electrochemical determination of dopamine, Analytical Methods, 4 (2012) 1725-1728.
[63] P. Wang, Y. Li, X. Huang, L. Wang, Fabrication of layer-by-layer modified multilayer films containing choline and gold nanoparticles and its sensing application for electrochemical determination of dopamine and uric acid, Talanta, 73 (2007) 431-437.
[64] T. Maiyalagan, J. Sundaramurthy, P.S. Kumar, P. Kannan, M. Opallo, S. Ramakrishna, Nanostructured [small alpha]-Fe2O3 platform for the electrochemical sensing of folic acid, Analyst, 138 (2013) 1779-1786.
[65] J.G. Velasco, Determination of standard rate constants for electrochemical irreversible processes from linear sweep voltammograms, Electroanalysis, 9 (1997) 880-882.
[66] R.S. Nicholson, I. Shain, Theory of Stationary Electrode Polarography. Single Scan and Cyclic Methods Applied to Reversible, Irreversible, and Kinetic Systems, Analytical Chemistry, 36 (1964) 706-723.

ACCEPTED MANUSCRIPT

[67] X. Wang, Z. You, Y. Cheng, H. Sha, G. Li, H. Zhu, W. Sun, Application of nanosized gold and graphene modified carbon ionic liquid electrode for the sensitive electrochemical determination of folic acid, Journal of Molecular Liquids, 204 (2015) 112-117.
[68] M. Mazloum-Ardakani, H. Beitollahi, M.K. Amini, F. Mirkhalaf, M. Abdollahi-Alibeik, New strategy for simultaneous and selective voltammetric determination of norepinephrine, acetaminophen and folic acid using ZrO2 nanoparticles-modified carbon paste electrode, Sensors and Actuators B: Chemical, 151 (2010) 243-249.
[69] R. Ojani, J.-B. Raoof, S. Zamani, Electrocatalytic Oxidation of Folic Acid on Carbon Paste Electrode Modified by Nickel Ions Dispersed into Poly(o-anisidine) Film, Electroanalysis, 21 (2009) 2634-2639.
[70] X.-l. Jiang, R. Li, J. Li, X. He, Electrochemical behavior and analytical determination of folic acid on carbon nanotube modified electrode, Russian Journal of Electrochemistry, 45 (2009) 772-777.
[71] H. Rajabi, M. Noroozifar, New synthesis of poly ortho-methoxyaniline nanostructures and its application to construct modified multi-wall carbon nanotube/graphite paste electrode for simultaneous determination of uric acid and folic acid, Materials Science and Engineering: C, 75 (2017) 791-797.
[72] A. Bard, L. Faulkner, Electrochemical Methods: Fundamentals and Applications, John Wiley & Sons, Inc2001.

ACCEPTED MANUSCRIPT

ACCEPTED MANUSCRIPT

Table 1: Redox peak potentials and currents for DA reaction at the surface of modified electrodes:

Modified electrode	E_{pa} (V)	E_{pc} (V)	ΔE_p (V)	I_{pa} (μA)	I_{pc} (μA)
bare GCE	0.700	-0.260	0.960	5.33	-4.103
POMA/GCE	0.523	-0.262	0.785	10.73	-8.022
Au/GCE	0.455	-0.186	0.641	12.00	-8.713
POMA-Au/GCE	0.330	-0.020	0.350	23.85	-19.98

ACCEPTED MANUSCRIPT

ACCEPTED MANUSCRIPT

Table 2: Comparison of the efficiency of some modified electrodes used in the electrocatalysis of DA.

Modified electrode	Method	LOD (μM)	LDR (μM)	References
HAu-G/GCE	CA	0.050	0.08-600	[58]
rGO/MWCNTs/AuNPs/GCE	ECL	0.067	0.2-70	[59]
HNP-AuAg alloy/GCE	CA	0.200	5-335	[60]
AuNPs/SDS-LDH/GCE	DPV	0.130	0.5-400	[61]
Gr/AuNps/GCE	DPV	1.860	5-1000	[62]
AuNPs/Ch/GCE	DPV	0.120	0.2-80	[63]
POMA-Au/GCE	DPV	0.062	10.0-300	Present Study

HAu-G/GCE: hollow gold-graphene nanocomposite modified GCE; *Gr/AuNps/GCE:* graphene-gold nanoparticles nanocomposite modified GCE; *rGO/MWCNTs/AuNPs/GCE:* reduced graphene oxide-multiwalled carbon nanotubes-gold nanoparticles modified GCE; *HNP-AuAg alloy/GCE:* hierarchical nanoporous AuAg alloy modified GCE; *AuNPs/Ch/GCE:* gold nanoparticles-choline modified GCE: *AuNPs/SDS-LDH/GCE:* gold nanoparticleslayered double hydroxide-sodium dodecyl sulphate; *CA:* chronoamperometry; *ECL:* Electrogenerated chemiluminescence; *DPV:* differential pulse voltammetry; *LOD:* limit of detection; *LDR:* linear dynamic range.

ACCEPTED MANUSCRIPT

ACCEPTED MANUSCRIPT

Table 3: Comparison of the efficiency of some modified electrodes used in the electrocatalysis of FA.

Modified electrode	Method	LOD (μM)	LDR (μM)	References
Mn-SnO_2/GCE	DPV	0.079	0.5-900	[3]
Au-ERGO/CILE	Amperometry	0.027	0.01-50	[67]
ZrO_2 nanoparticles/CPE	DPV	0.089	10-2000	[68]
Ni-POA/CPE	CV	91.000	100–5000	[69]
MWCNT/GCE	Stripping voltammetry	0.130	0.3-80	[70]
POMANS-MWCNT/GPE	LSV	0.113	0.5-68	[71]
POMA-Au/GCE	DPV	0.090	0.5-900	Present Study

Au-ERGO/CILE: gold nanoparticles-electrochemical reduced graphene oxide modified carbon ionic liquid electrode; *ZrO_2 nanoparticles/CPE:* ZrO_2 nanoparticles modified carbon paste electrode; *Ni-POA/CPE:* nickel modified poly(o-anisidine) carbon paste electrode; *MWCNT/GCE:* multiwalled carbon nanotubes modified GCE; *POMANS-MWCNT/GPE:* poly(o-methoxyanline)-multiwalled carbon nanotubes modified graphite paste electrode; *Mn-SnO_2/GCE:* Mn doped SnO_2 modified GCE; *CV:* cyclic voltammetry; *LSV*: linear sweep voltammetry.

ACCEPTED MANUSCRIPT

ACCEPTED MANUSCRIPT

Table 4: Recovery tests of DA and FA in pharmaceutical samples (n=3) using POMA-Au/GCE sensor.

Sample	Added (μM)	Expected (μM)	Found (μM)[a]	Recovery (%)
DA Injection	10	10	9.73±0.41	97.3
	20	20	19.54±0.24	97.7
	30	30	30.06±0.35	100.2
Folvite	10	10	9.87±0.16	98.7
	20	20	19.92±0.37	99.6
	30	30	29.14±0.63	97.1

[a]: Average of three measurements; ±: represents the standard deviation.

ACCEPTED MANUSCRIPT

ACCEPTED MANUSCRIPT

Table 5. Recovery tests of DA and FA in human urine samples (n=3) using POMA-Au/GCE sensor.

Sample	Added (μM)		Found (μM) [a]		Recovery ((%)	
	DA	FA	DA	FA	DA	FA
Human Urine	5	5	4.89±0.31	4.95±0.12	97.8	99.0
	10	10	9.75±0.22	9.62±0.17	97.5	96.2
	15	15	14.85±0.11	14.77±0.24	99.0	98.5
	20	20	19.86±0.25	19.74±0.53	99.3	98.7

[a]: Average of three measurements; ±: represents the standard deviation.

ACCEPTED MANUSCRIPT

ACCEPTED MANUSCRIPT

Highlights

- Simultaneous determination of DA and FA was studied using POMA-Au nanocomposite.
- The nanocomposite was characterized by XRD, XPS and HRTEM.
- The important electrochemical parameters of DA and FA were determined.
- The practicality of the POMA-Au/GCE sensor has been determined.

ACCEPTED MANUSCRIPT

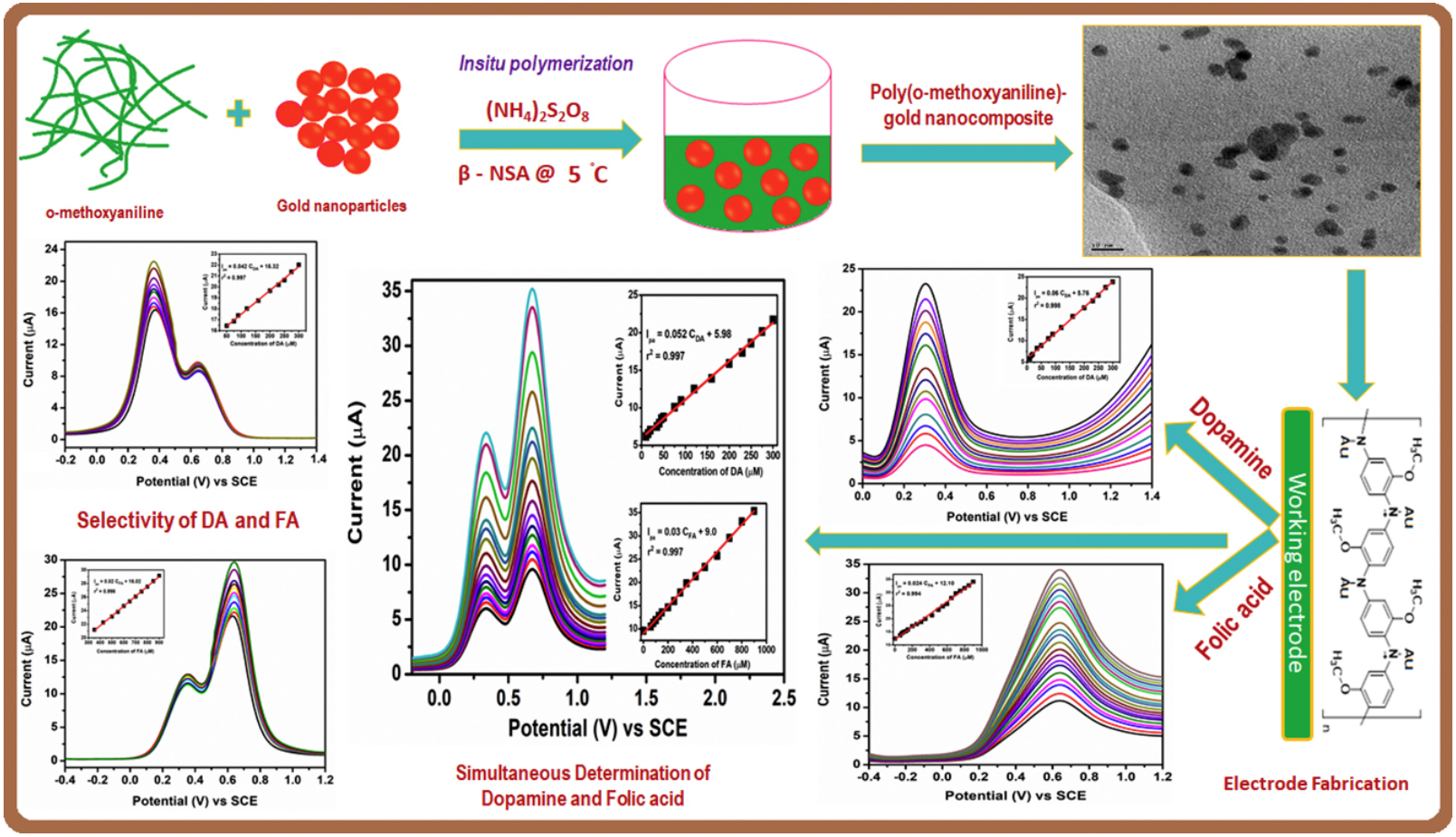

Graphics Abstract

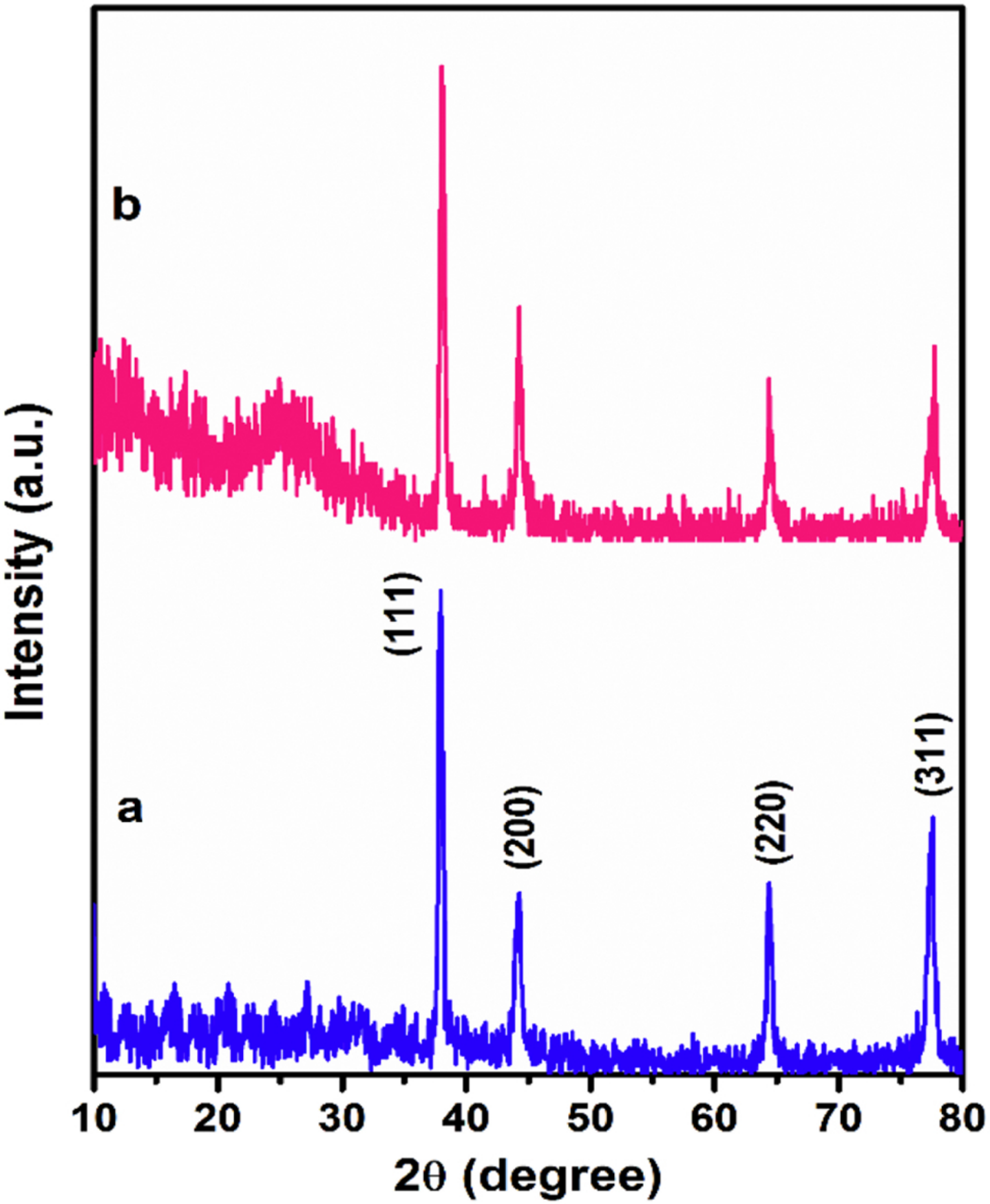

Figure 1

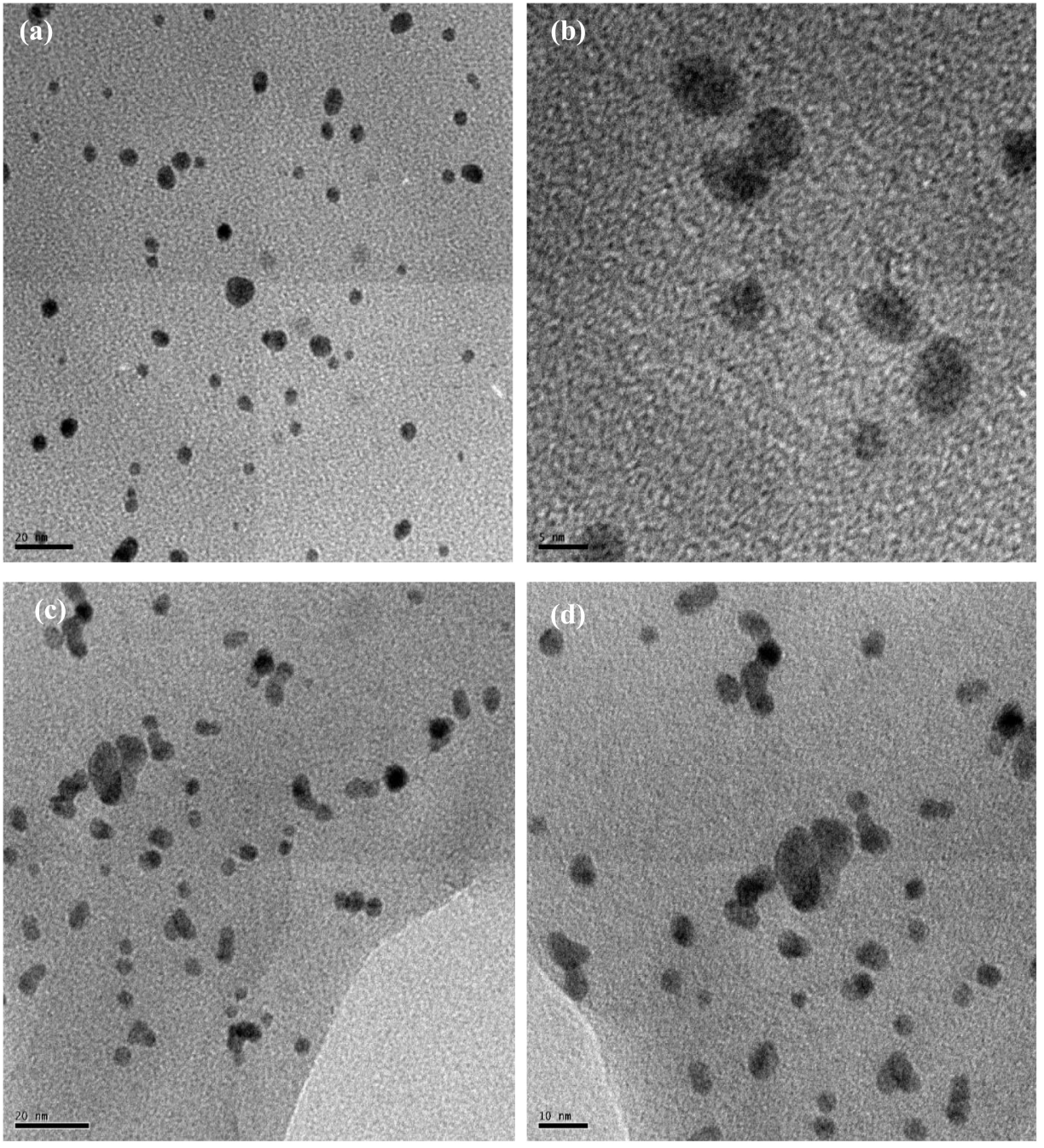

Figure 2ad

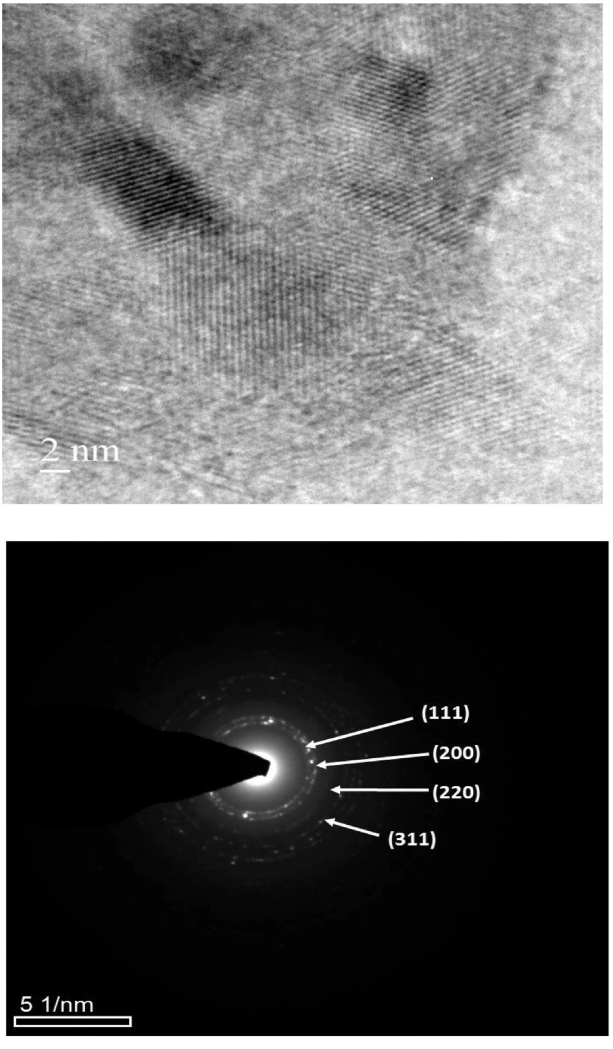

Figure 2ef

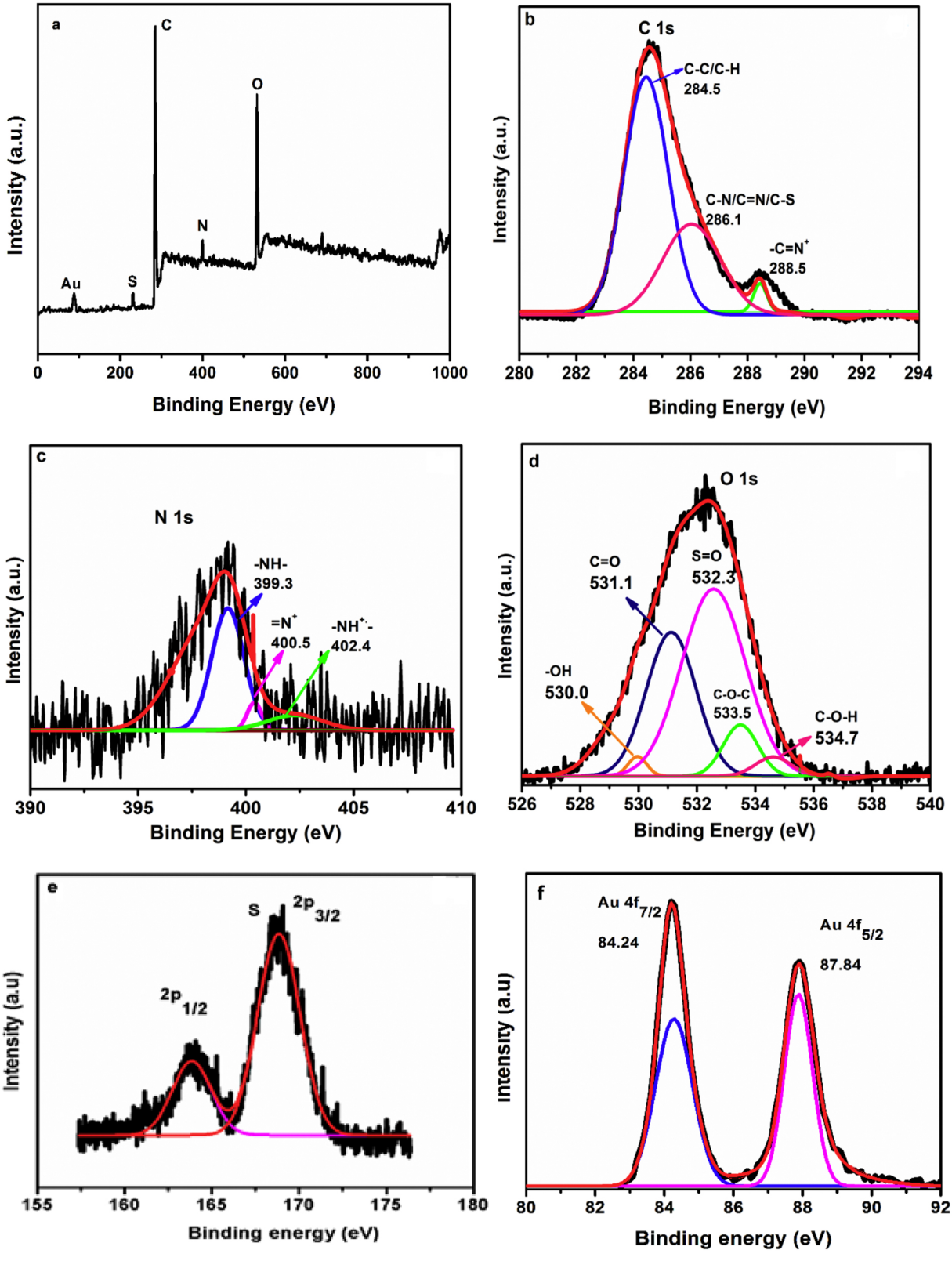
a
C
O
N
Au
S
Intensity (a.u.)
0
200
400
600
800
1000
Binding Energy (eV)
b
C 1s
C-C/C-H
284.5
C-N/C=N/C-S
286.1
-C=N+
288.5
Intensity (a.u.)
280
282
284
286
288
290
292
294
Binding Energy (eV)
c
N 1s
-NH-
399.3
=N+
400.5
-NH+·-
402.4
Intensity (a.u.)
390
395
400
405
410
Binding Energy (eV)
d
O 1s
C=O
531.1
S=O
532.3
-OH
530.0
C-O-C
533.5
C-O-H
534.7
Intensity (a.u.)
526
528
530
532
534
536
538
540
Binding Energy (eV)
e
S
2p3/2
2p1/2
Intensity (a.u)
155
160
165
170
175
180
Binding energy (eV)
f
Au 4f7/2
84.24
Au 4f5/2
87.84
Intensity (a.u)
80
82
84
86
88
90
92
Binding energy (eV)

Figure 3

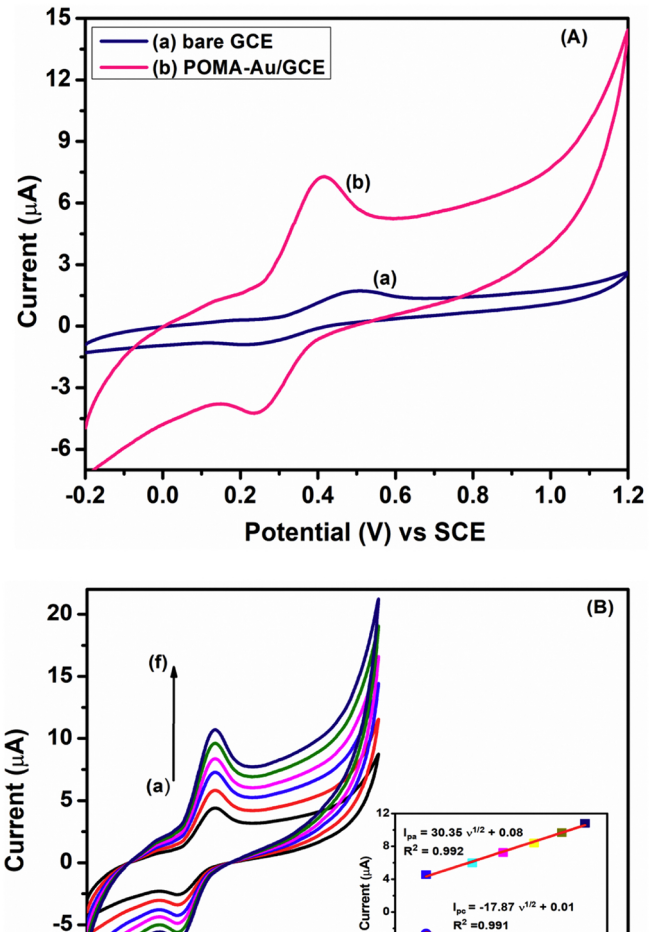
(a) bare GCE
(b) POMA-Au/GCE
(A)
(b)
(a)
Current (μA)
Potential (V) vs SCE
(B)
(f)
(a)
Current (μA)
Potential (V) vs SCE
I_{pa} = 30.35 $\nu^{1/2}$ + 0.08
R^2 = 0.992
I_{pc} = -17.87 $\nu^{1/2}$ + 0.01
R^2 =0.991
Current (μA)
$\nu^{1/2}$ ($V^{1/2}$ $s^{-1/2}$)

Figure 4

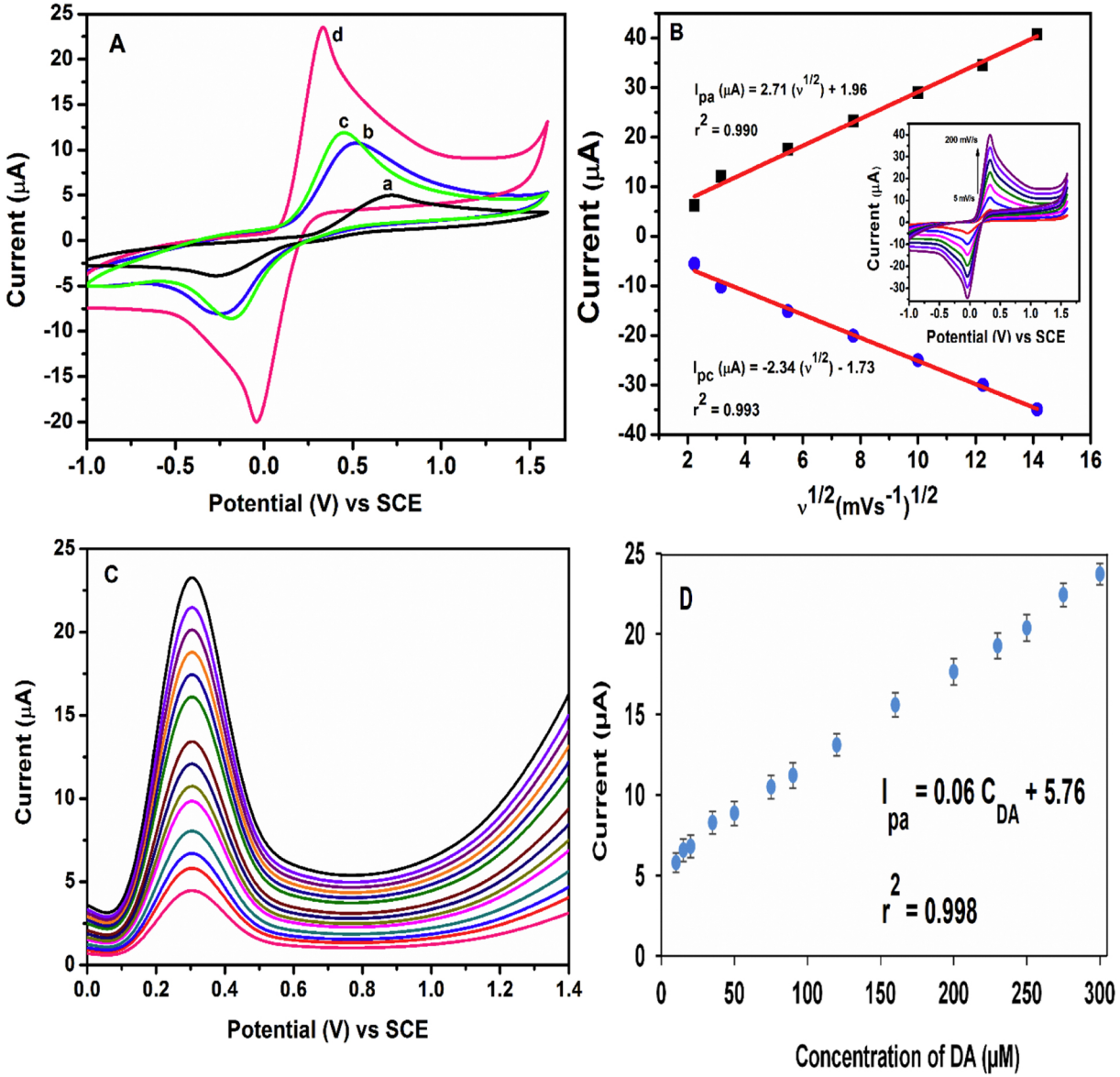
A
d
c
b
a
Current (μA)
Potential (V) vs SCE
B
I_{pa} (μA) = 2.71 ($\nu^{1/2}$) + 1.96
r^2 = 0.990
I_{pc} (μA) = -2.34 ($\nu^{1/2}$) - 1.73
r^2 = 0.993
200 mV/s
5 mV/s
Current (μA)
Potential (V) vs SCE
Current (μA)
$\nu^{1/2}$(mVs^{-1})$^{1/2}$
C
Current (μA)
Potential (V) vs SCE
D
I_{pa} = 0.06 C_{DA} + 5.76
r^2 = 0.998
Current (μA)
Concentration of DA (μM)

Figure 5

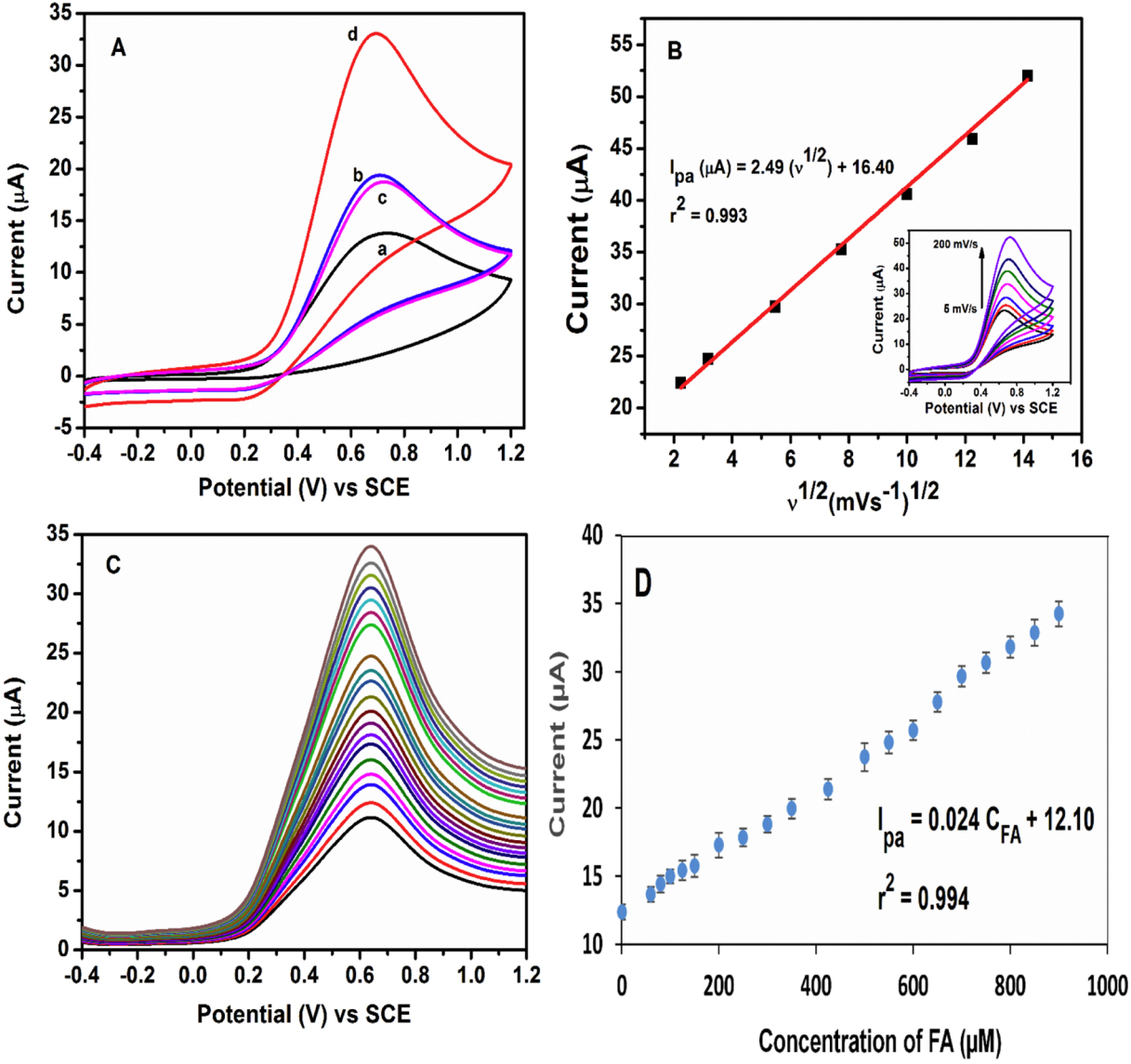
A
d
b
c
a
Current (μA)
Potential (V) vs SCE
B
I_{pa} (μA) = 2.49 ($\nu^{1/2}$) + 16.40
r^2 = 0.993
200 mV/s
5 mV/s
Current (μA)
Potential (V) vs SCE
Current (μA)
$\nu^{1/2}(mVs^{-1})^{1/2}$
C
Current (μA)
Potential (V) vs SCE
D
Current (μA)
I_{pa} = 0.024 C_{FA} + 12.10
r^2 = 0.994
Concentration of FA (μM)

Figure 6

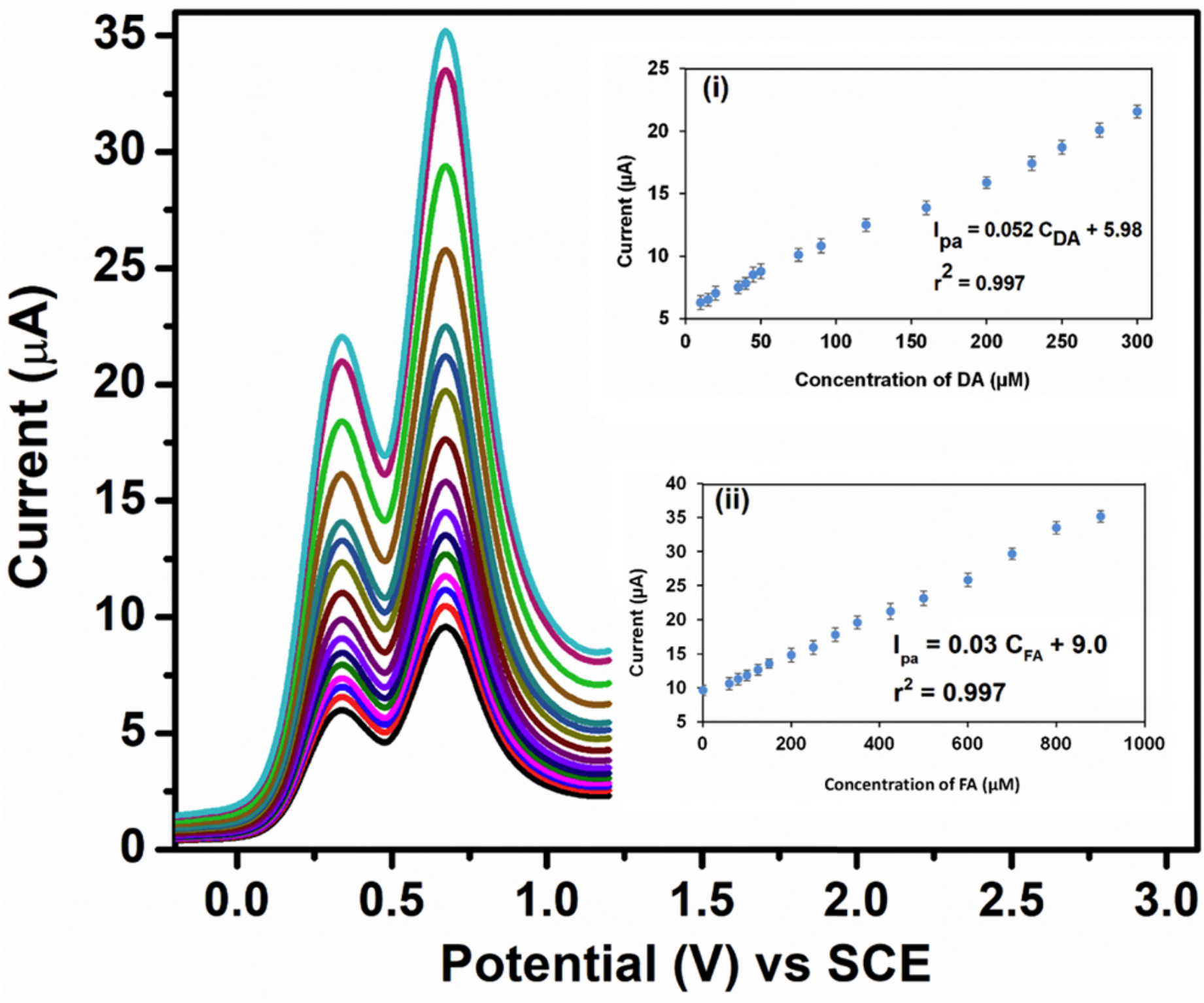
Current (μA)
Potential (V) vs SCE
(i)
Current (μA)
Concentration of DA (μM)
I_{pa} = 0.052 C_{DA} + 5.98
r^2 = 0.997
(ii)
Current (μA)
Concentration of FA (μM)
I_{pa} = 0.03 C_{FA} + 9.0
r^2 = 0.997

Figure 7

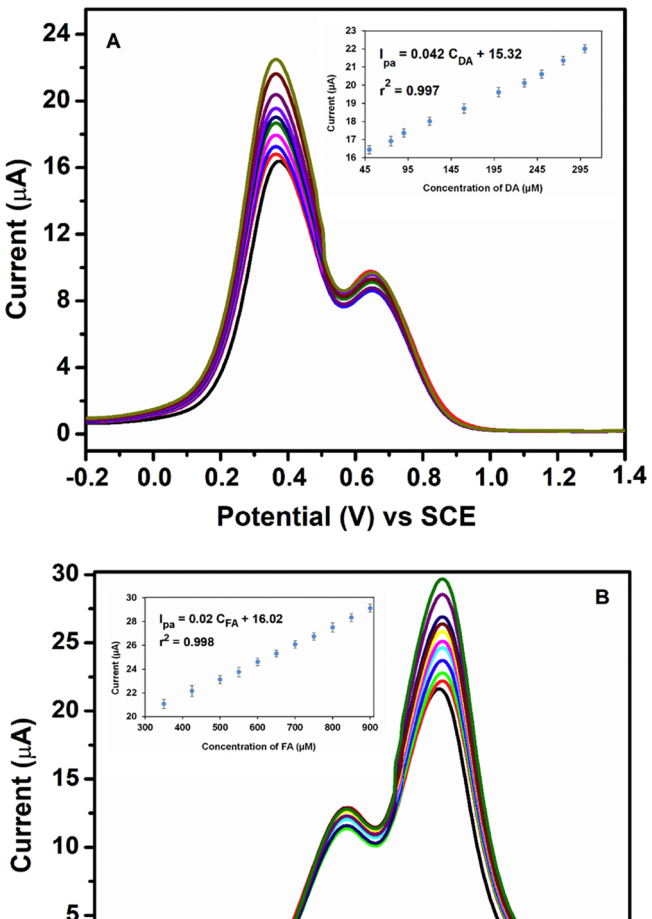
A
I_{pa} = 0.042 C_{DA} + 15.32
r^2 = 0.997
Current (μA)
Concentration of DA (μM)
Current (μA)
Potential (V) vs SCE
B
I_{pa} = 0.02 C_{FA} + 16.02
r^2 = 0.998
Current (μA)
Concentration of FA (μM)
Current (μA)
Potential (V) vs SCE

Figure 8

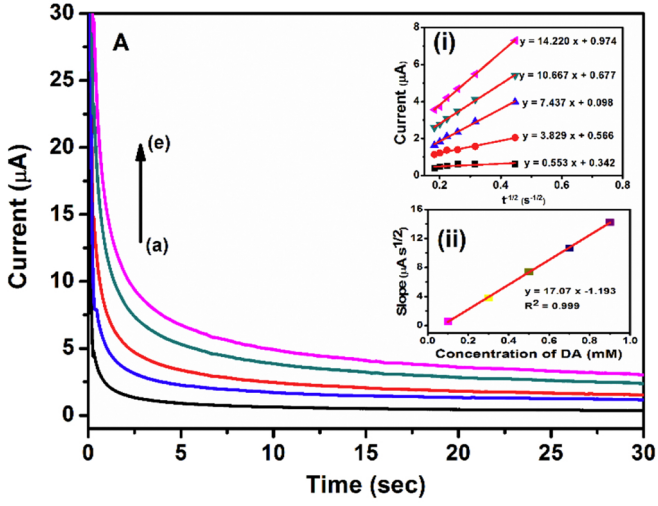
A
(e)
(a)
Current (μA)
Time (sec)
(i)
y = 14.220 x + 0.974
y = 10.667 x + 0.677
y = 7.437 x + 0.098
y = 3.829 x + 0.566
y = 0.553 x + 0.342
Current (μA)
t^-1/2 (s^-1/2)
(ii)
y = 17.07 x -1.193
R^2 = 0.999
Slope (μA s^1/2)
Concentration of DA (mM)

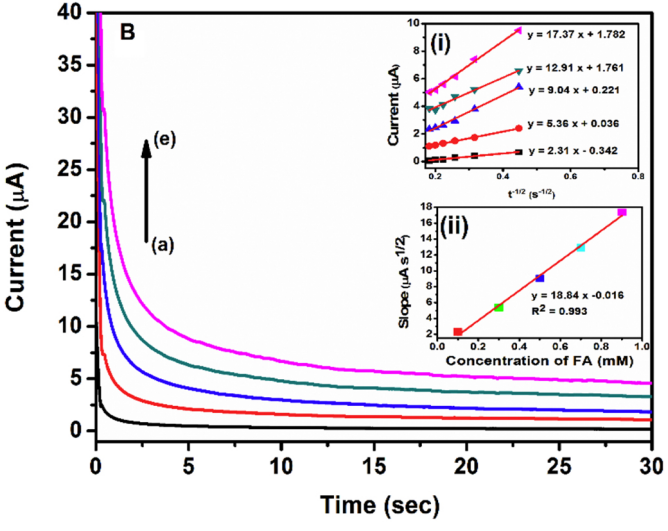
B
(e)
(a)
Current (μA)
Time (sec)
(i)
y = 17.37 x + 1.782
y = 12.91 x + 1.761
y = 9.04 x + 0.221
y = 5.36 x + 0.036
y = 2.31 x - 0.342
Current (μA)
t^-1/2 (s^-1/2)
(ii)
y = 18.84 x -0.016
R^2 = 0.993
Slope (μA s^1/2)
Concentration of FA (mM)

Figure 9